Chapter 22

Piezoelectric Plate Sensor (PEPS) for Analysis of Specific *KRAS* Point Mutations at Low Copy Number in Urine Without DNA Isolation or Amplification

Ceyhun E. Kirimli, Wei-Heng Shih, and Wan Y. Shih

Abstract

We have examined in situ detection of single-nucleotide *KRAS* mutations in urine using a $(Pb(Mg_{1/3}Nb_{2/3})O_3)_{0.65}(PbTiO_3)_{0.35}$ (PMN-PT) piezoelectric plate sensor (PEPS) coated with a 17-nucleotide (nt) locked nucleic acid (LNA) probe DNA complementary to the *KRAS* mutation without DNA isolation and amplification. In situ mutant (MT) DNA in urine in a wild type (WT) background was carried out at a flow rate of 4 mL/min and at 63 °C with the PEPS vertically situated at the center of the flow. Both the temperature and the impingement flow force discriminated the wild type. Under these conditions PEPS was shown to specifically detect *KRAS* MT in situ within 30 min with an analytical sensitivity of 60 copies/mL in a clinically relevant background of WT with concentrations 1000-fold greater than that of MT without DNA isolation, amplification, or labeling. For validation, detection was performed in a mixture of blue MT fluorescent reporter microspheres (FRMs) (MT FRMs) that bound to only the captured MT, and orange WT FRMs that bound to only the captured WT. The captured blue MT FRMs still outnumbered the orange WT FRMs by a factor of 4–1 even though WT was 1000-fold of MT in urine, illustrating the specificity of the point mutation detection.

Keywords Piezoelectric plate sensor, Piezoelectric sensor, Biosensor, Amplification-free hybridization detection, Cell-free point-mutation detection

1 Introduction

A lead magnesium niobate–lead titanate $(Pb(Mg_{1/3}Nb_{2/3})O_3)_{0.65}(PbTiO_3)_{0.35}$ (PMN-PT) piezoelectric plate sensor (PEPS) consisting of an 8-μm thin highly piezoelectric PMN-PT layer made without a substrate (*see* Fig. 1a, c) [1, 2] is a unique sensor with polymerase chain reaction (PCR)-like 100 zM (10^{-19} M or 60 copies/mL) analytical sensitivity in label-free DNA detection without DNA isolation, concentration, and amplification. [3] With receptor immobilized on the surface, binding of a target DNA decreased the resonance frequency (f) of the PEPS. Label-free

Ben Prickril and Avraham Rasooly (eds.), *Biosensors and Biodetection: Methods and Protocols, Volume 2: Electrochemical, Bioelectronic, Piezoelectric, Cellular and Molecular Biosensors*, Methods in Molecular Biology, vol. 1572,
DOI 10.1007/978-1-4939-6911-1_22,

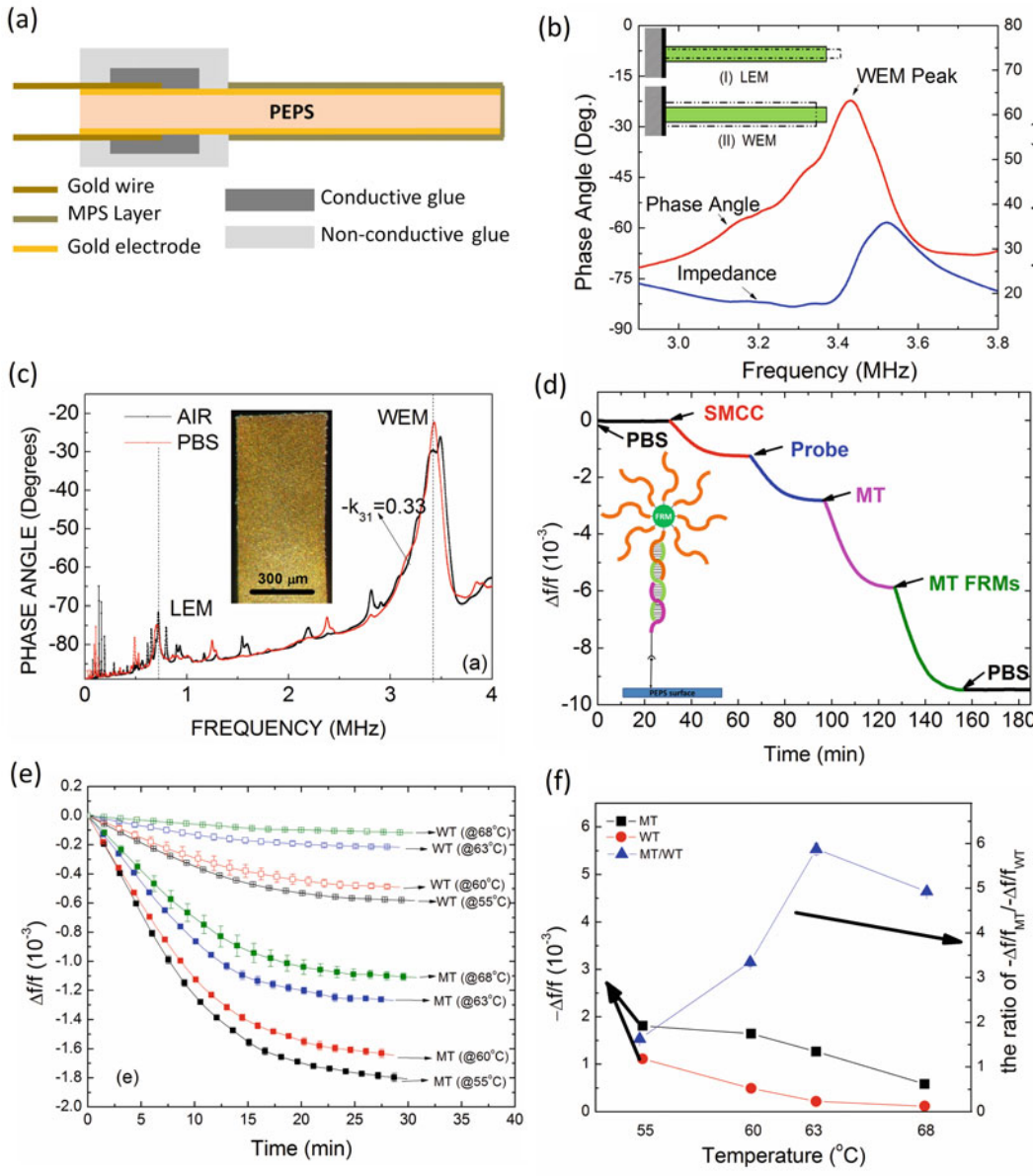

Fig. 1 (**a**) A schematic of the side view of the PEPS. The gold wires were connected to the top and bottom gold electrodes with conductive glue. The entire rear end, including the conductive glue, was covered with non-conductive glues. MPS layer covered the front end of the PEPS that was not covered by the nonconductive glue. (**b**) Blowup of both the impedance-versus-frequency (*blue*) and phase angle-versus-frequency (*red*) spectra around the WEM resonance peak around 3.4 MHz. Also included are schematics for LEM and WEM vibrations in insert (I) and (II), respectively. (**c**) In-air (*black*) and in-PBS (*red*) phase angle-versus-frequency resonance spectra with an insert showing an optical micrograph of the PEPS, and (**d**) relative resonance frequency shift, $\Delta f/f$, of the PMN-PT PEPS going through PBS step (0–30 min), the SMCC bonding step (30–60 min), the probe immobilization step(60–90 min), the MT detection step (90–120 min), the MT FRMs detection step (120–150 min), and the final PBS step (150–180 min) with an insert showing a schematic of the molecules involved in these steps. (**e**) MT (solid symbols) and WT (open symbols) detection at 1×10^{-15} M in PBS at 55 °C (*black*), 60 °C (*red*), 63 °C (*blue*), and 68 °C (*green*) for 30 min, (**f**) average $-\Delta f/f$ at 25–30 min versus temperature, squares for MT and circles for WT. Also plotted is the ratio of the average $-\Delta f/f$ at 25–30 min of the MT to that of the WT (triangles) (the right side of the double-y plot)

detection of the target DNA in situ was quantified by measuring this frequency decrease (Δf) using simple and inexpensive electrical means. What is unique about PMN-PT PEPS is its ability to inherently enhance the detection resonance frequency shift by more than 1000 times by the polarization orientation switching within the piezoelectric layer, which was induced by the surface stress generated by the binding of the target analyte on the PEPS surface [4–9]. This enhancement is further amplified in DNA detection as the stress generated by a highly negatively charged DNA molecule to an already highly negatively charged probe DNA layer is drastically higher than that of a protein molecule to a charge-neutral antibody layer. As a result, PEPS exhibits unprecedented sensitivity in direct DNA detection without the need of DNA extraction, concentration, or amplification. [3, 8, 10] "Hard" piezoelectric devises such as QCM and SAW have no switchable polarization thus no such enhancement [11]. In PZT PEMS (another piezoelectric sensor pioneered by Shih and Shih that also exhibit polarization switching-enhanced Δf/f) the enhancement was ten times smaller [12–16] than PMN-PT PEPS due to substrate pinning in thin PZT PEMS (1 μm) on a silicon substrate [14–16] that minimized polarization switching or the thickness (127 μm) of the PZT layer in thick PZT PEMS made of commercial PZT [12, 13, 17] because the enhancement is inversely proportional to the thickness [6].

Gene mutation is an important form of genetic defects that play a central role in cancer pathways. Detecting gene mutation is essential for cancer diagnosis, therapy decision, and therapy efficacy monitoring. The challenge for gene sequencing from solid tumor samples is that therapeutic decision making based on a single biopsy can be very difficult due to tumor heterogeneity [18]. Furthermore, the biopsy procedures used for removing tissues from cancers of the internal organs are highly intrusive and expensive and not performed in some cases due to the increased risk of tumor seeding to other sites [19]. These shortcomings make it highly desirable if body fluids such as blood or urine can be used for cancer genetic marker detection.

PCR has been the method of detecting circulating deoxyribonucleic acid (DNA) markers in serum or urine. To detect gene mutation, PCR is typically followed with melting temperature analysis to differentiate mutant (MT) from the wild type (WT), the normal form of the gene. So far, detecting mutations in sera or urine has been challenging because (1) the melting-temperature difference between a single-nucleotide MT and the WT can be only a few degrees [20], (2) the concentrations of circulating MT markers are exceedingly low (much lower than 10^{-18} M or 600 copies/mL) [21], (3) circulating MT markers are typically outnumbered by the WT by a factor of 240 or larger [22], and (4) transrenal DNA exist in urine in the form of short fragments often less than 200 base pairs (bp) [23], and PCR suffers from amplicon size, where

only a small amount of the naturally occurring fragments in urine can be amplified [22, 24]. These combinations make it difficult to detect circulating mutations sensitively and specifically. Therefore, if there is a genetic detection method that can detect genetic mutations in short DNA fragments of less than 200 bp at concentrations lower than aM (10^{-18} M) and in a background of more than 240-fold wild type (WT) without the need of DNA isolation or amplification it would be ideal for reliably detecting circulating genetic mutations in urine that can greatly help cancer diagnostics and treatment decision and monitoring.

In an earlier study, we have shown that flow can create a force to impinge on the DNA bound on the probe on the sensor surface [25]. Because the probe is complementary to MT but not WT the bonding of WT to the probe is weaker than that of MT to the probe. As a result, less WT will remain bound on the probe than MT by the flow impingement force. We have shown that detect MT in a flow by controlling the flow speed together with temperature is more specific than detecting MT by controlling the temperature alone without a flow [25]. In fact, by controlling the flow rate and temperature, PEPS was shown capable of detecting a double mutation, hepatitis B virus double mutation (HBVDM), in a background of 250-fold WT in a flow and in situ [26]. Since it is harder to detect a point mutation than a double mutation against the WT it would be of interest to examine if using similar flow speed and temperature controls one could also detect point mutations with high specificity against the WT for circulating mutation detection applications where the WT outnumbers the MT by more than 240-fold [22].

KRAS mutations are point (single-nucleotide) mutations (PMs) at codons 12 and 13 and less frequently at codon 61 that occur in about 50% of colorectal cancers [27] and more than 80% of pancreatic cancers [28]. In this study investigate in situ detection of *KRAS* point mutation (PM) in urine against the WT in real time using a PEPS coated with locked nucleic acid (LNA) probe in a flow and with temperature control but without DNA isolation or amplification. Among the seven most common *KRAS* mutations, codon-12 GGT to GTT point mutation (Glycine to Valine) (G12 V) is associated with a higher mortality rate [29]. Frequency of this mutation among *KRAS* mutated colorectal cancers is 21.9–24.4% [30]. We will use the *KRAS* G12 V PM as the model PM. Specifically, we will use a 50-nt *KRAS* PM as the model MT. To increase the melting-temperature difference between the MT and WT and enhance the specificity of mutation detection [31–38], we have designed and immobilized an LNA-containing probe on the PEPS surface and carried out in situ *KRAS* PM MT detection against the WT at a temperature below the melting temperature of the MT but above that of the WT and with a flow rate of 4 mL/min. We showed that the PEPS positively and specifically detected

the *KRAS* G12 V PM MT at a concentration of 60 copies/mL (100zM, or 10^{-19} M) in a background of 1000-fold WT and further validated the MT detection by following with in situ fluorescent reporter microspheres (FRMs) detection and by visualizing the fluorescent colors of FRMs. The numbers of captured MT FRMs outnumbered the captured WT FRMs by a factor of 4 to 1, indicating the specificity of PEPS single-nucleotide PM detection even when the samples contains 1000-fold WT.

2 Materials

1. The probe is a single-stranded 17-nt LNA probe synthesized by Exiqon as shown in Table 1.
2. The MT, a 50-nt single-stranded DNA, containing the sequence complementary to the probe, plus 33 nt of the immediately upstream sequence as shown in Table 1 was synthesized by Sigma.
3. The WT, a 50-nt long single-stranded DNA, containing the sequence complementary to the probe except for the point mismatch plus 33 nt of the immediately downstream sequence as shown in Table 1 was synthesized by Sigma.
4. MTrDNA, a single-stranded DNA complementary to the 33-nt upstream sequence of the MT, which was amine-activated with a 7-PEG spacer at the 3′ end to be conjugated to MT FRMs as shown in Table 1 was synthesized by Sigma.

Table 1
Sequences of the probe, MT, WT, MTrDNA, and the WTrDNA and the melting temperatures (T_m) of MT with probe, WT with probe, MTrDNA with MT, and WTrDNA with WT

Type of DNA	Sequence (5′→3′)	T_m
Probe(17 nt)	Amine-(PEG)12-TGGAGCTG***T***TGGCGTAG	–
MT(50 nt)	TCTGAATTAGCTGTATCGTCAAGGCACTCTTGCC TACGCCA***A***CAGCTCCA	70 °C (Probe to MT
WT(50 nt)	CTACGCCA***C***CAGCTCCAACTACCACAAGTTTATATT CAGTCATTTTCAGC	55 °C (Probe to WT)
MTrDNA (33 nt)	GCAAGAGTGCCTTGACGATACAGC TAATTCAGA-(PEG)7-Amine	78.5 °C (MTrDNA to MT)
WTrDNA (33 nt)	Amine-(PEG)12- GCTGAAAATGACTGAATATAAACTTGTGGTAGT	73.6 °C (WTrDNA to WT)

Note that the site where the mutation occurs is italic and bold in the MT, WT, and probe and the LNA bases in the probe are underlined. The melting temperatures were estimated using a 115 mM salt concentration consistent with urinary salt content [39, 40] and a LNA/DNA concentration of 50 nM.

5. WTrDNA, a single-stranded DNA complementary to the 33-nt downstream sequence of the WT, which was amine-activated with a 12-PEG spacer at the 5′ end to be conjugated to WT FRMs as shown in Table 1 was synthesized by Sigma.
6. MT FRMs which emitted blue light (Bright Blue (BB) (≅ Coumarin)) with excitation maximum at 360 nm and emission maximum at 407 nm was synthesized by Polysciences.
7. WT FRMS, which emitted yellow-green light (Yellow Green (YG) (≅ Fluorescein)) with excitation maximum at 441 nm and emission maximum at 486 nm was synthesized by Polysciences.
8. Thermal evaporation (Thermionics VE 90).
9. Wire saw cutting (Princeton Scientific Precision, Princeton, NJ).
10. Conductive glue ((XCE 3104XL, Emerson and Cuming Company, Billerica, MA).
11. Nonconductive glue (Loctite 1C Hysol Epoxy Adhesive).
12. Bovine serum albumin (BSA) (Sigma).
13. 3-mercaptopropyltrimethoxysilane (MPS) (Sigma).
14. Sulfosuccinimidyl-4-(N-maleimidomethyl)cyclohexane-1-carboxylate (sulfo-SMCC) (Pierce).
15. Incubator (Digital Control Steel Door Incubator 10-180E, Quincy Lab).
16. Agilent 4294A electrical impedance analyzer (Agilent Technologies).
17. Resonance spectra and resonance frequency shift with time during detection were measured by a portable AIM 4170 C impedance analyzer (Array Solutions).
18. Peristaltic pump (Cole-Parmer 77,120–62).
19. Fluorescence Imaging was carried out using a fluorescence microscope (Olympus BX51).
20. Gold nuggets for thermal evaporation of gold electrodes (Lesker).
21. Chromium nuggets for thermal evaporation of chromium bonding layers before gold deposition (Lesker).
22. Gold wires (Kulicke & Soffa).
23. Glass substrate (Fisher).
24. D350/50, D460/50 filter, HQ545/30 and 400 nm long-pass filter (Chroma).
25. MatLab (MathWorks).
26. Material for flow cell fabrication is polycarbonate (Interstate Plastics).
27. Nb_2O_5 (99.99%, Aldrich), $Mg(NO_3)_2{\cdot}6H_2O$ (Aldrich).

28. Titanium isopropoxide ($Ti(OCH(CH_3)_2)_4$, 99.9% Alfa Aesar).
29. Lead acetate anhydrous ($Pb(CH_3COO)_2.2Pb(OH)_2$, Fluka, St. Louis, MO).
30. NH_4OH (5 M, Aldrich).
31. Ultrasonication (50 MHz, 50 W, Ultrasonic Homogenizer 4710 series, Cole-Parmer Instrument Co., Vernon Hills, IL).
32. Ethylene glycol (EG) ($HOCH_2CH_2OH$, Alfa Aesar, Ward Hill, MA).
33. Hotplate (Cole-Parmer), Furnace (Carbolite).
34. Ball milling machine (Paul O. Abbe).
35. Doctor blade (Tape Casting Warehouse, Morrisville, PA).
36. Mylar film (Tape Casting Warehouse, Morrisville, PA).
37. Ethanol (Fisher), phosphate buffer saline solution (Fisher).
38. 1-ethyl-3-(3-dimethylaminopropyl) carbodiimide (EDC) (Pierce), sulfonated *N*-hydroxysuccinimide (sulfo-NHS) (Pierce).

3 Methods

3.1 Fabrication of PMN-PT Freestanding Film

1. $[Pb(Mg_{1/3}Nb_{2/3})O_3]_{0.65}[PbTiO_3]_{0.35}$ (PMN-PT) powder was synthesized using a double precursor coating approach [2] First, 5.38 g of $Mg(NO_3)_2{\cdot}6H_2O$ were dissolved in 100 mL of DI water and 5.26 g of Nb_2O_5 powder were added to the solution and ultra-sonicate for 10 min to break up the Nb_2O_5 agglomerates. To precipitate $Mg(OH)_2$ on the Nb_2O_5 surface, a tenfold diluted NH_4OH solution was added to the suspension dropwise until the pH was 10.5 followed by continuous stirring for 30 min.
2. The suspension was then dried at 150 °C on a hotplate.
3. After drying, the $Mg(OH)_2$-coated Nb_2O_5 powder was suspended in a lead acetate anhydrous solution in ethylene glycol (EG) with 15% excess lead.
4. The suspension was then dried at 230 °C on a hotplate.
5. The dried powder was calcined in a furnace at 800 °C for 2 h to obtain crystalline lead magnesium niobate (PMN).
6. The obtained PMN powder was suspended in an EG solution of lead titanate (PT) precursor solution with containing lead acetate anhydrous and titanium isopropoxide and ball milled for 24 h.

7. The ball-milled powder was dried at 230 °C on a hotplate followed by heat treatment at a rate of 1 °C/min to 500 °C in a furnace for 2 h to burn out the organics.
8. The obtained powder was then dried and ball-milled with proprietary dispersants, binders, and plasticizers for 48 h to obtain the slurry for tape casting.
9. The slurry was then poured in a doctor blade to cast the green tape on a mylar film.
10. The green tape was then heated in a furnace at 500 °C for 4 h to burn out the organics followed by sintering in a furnace at 1175 °C for 2 h.

3.2 PEPS Fabrication and Electrical Insulation

1. The PEPS was 1.2 mm long and 0.45 mm wide fabricated from $(PbMg_{1/3}Nb_{2/3}O_3)_{0.65}$-$(PbTiO_3)_{0.35}$ (PMN-PT) freestanding films 8 μm thickness that was coated with 110 nm thick Cr/Au electrode by thermal evaporation cut into 2.5 mm by 0.45 mm strips by a wire saw as shown in the insert of Fig. 1c.
2. Gold wires, 10 μm in diameter, were glued to the top and bottom electrodes of each strip using conductive glue.
3. The rear end of the strip was fixed on a glass substrate by a nonconductive glue to form the PEPS geometry and the piezoelectric properties of the sensor was realized by aligning the polarization (poling) with an electric field of 15KV/cm at 90 °C for 60 min in an incubator.
4. The relative dielectric constant of the PEPS was measured to be about 1800 using an Agilent 4294A electrical impedance analyzer, with a loss factor of 2.8% at 1 kHz.
5. The PEPS was electrically insulated to stabilize the resonance peaks for in-liquid detection by using a new MPS solutions coating scheme involving enhanced MPS cross-linking at pH = 9.0 with 0.1% of MPS and 0.5% of water in ethanol [41]. The coating solution was replaced with a fresh one every 12 h until the resonance peak frequency was stable in phosphate saline buffer (PBS) solution.
6. The MPS insulation also served as the anchor to immobilize the probe via the bifunctional linker sulfo-SMCC. The pKa of thiols is about 10.5. Under the coating conditions at pH = 9.0 or the immobilization conditions at pH = 7, most of the thiols were unoxidized and good for the immobilization because maleimides of the sulfo-SMCC reacted with sulfhydryl groups at pH 6.5–7.5 to form stable thioether bonds.
7. A schematic of length extension mode (LEM) vibrations and that of width extension mode (WEM) vibrations of a PEPS are shown in the insert (I) and (II) of Fig. 1b, respectively. The impedance (blue) and phase angle (red) versus frequency

resonance spectra around the first WEM peak frequency—which was taken as the peak frequency of the phase angle versus frequency spectrum—are shown in Fig. 1b. Because the phase-angle resonance spectrum was much more symmetric than that of the impedance, all the following detections were carried out using the phase-angle spectrum to track the WEM peak. At a given time, the frequency of the resonance peak was determine by first smooth the resonance peak by adjacent averaging followed by fitting the smoothed curve to more than 50 palabras of different frequency ranges and averaging over the all of the fitted resonance frequencies.

3.3 Probe Immobilization, Nonspecific Binding Blocking, and FRMs Conjugation

1. The probe is complementary to the sequence of the *KRAS* gene (Gene ID: 3845) centered around the *KRAS* G12 V PM with the 3 LNA bases also centred around the PM and amine-activated with a 12-polyethyleneglycol (PEG) spacer at the 5′ end.
2. With the 3 LNA bases, the melting temperature for the probe with the MT was 70 °C and that for probe with the WT 55 °C. The difference between the melting temperature of the probe with the MT and that of probe with the WT was thus increased from 10 to 15 °C (*see* **Note 1**).
3. Sulfo-SMCC was dissolved in water followed by dilution in a phosphate buffer saline (PBS) solution to 5 mM concentration. To immobilize the amine-activated probe on the PEPS surface, the MPS-coated PEPS was first immersed in 200 μL of a 5 mM sulfo-SMCC solution in PBS with the pH adjusted to 6.5 for 1 h. This would allow the maleimides of the sulfo-SMCC reacted with sulfhydryl groups on the MPS to form stable thioether bonds. The sensor was then washed three times with deionized water and then it was immersed in a solution of 10 μM amine activated probe dissolved in 200 μL of PBS (pH 8.0). The NHS-ester of the sulfo SMCC reacted with the amine group of the probe to form a peptide bond.
4. The probe immobilized on the MPS surface was quantified to be about 1.9 probes/nm^2 using a 5-MHz quartz crystal microbalance (QCM) [42]. In the QCM test, the sulfo-SMCC and probe binding steps resulted in 15 Hz and 120 Hz resonance frequency shifts, respectively. This corresponds to an adsorbed sulfo-SMCC layer of 0.9×10^{-7} g/cm^2 and an adsorbed probe layer 7.2×10^{-7} g/cm^2 as calculated using the Sauerbrey equation. With the molecular weights of sulfo-SMCC and that of the probe being 436 and 4938 g/mol, respectively, these results corresponded to an adsorbed sulfo-SMCC layer with a density of 2.7 molecules/nm^2 upon which a probe layer immobilized with a density of 1.9 molecules/nm^2. Thus, the SH of

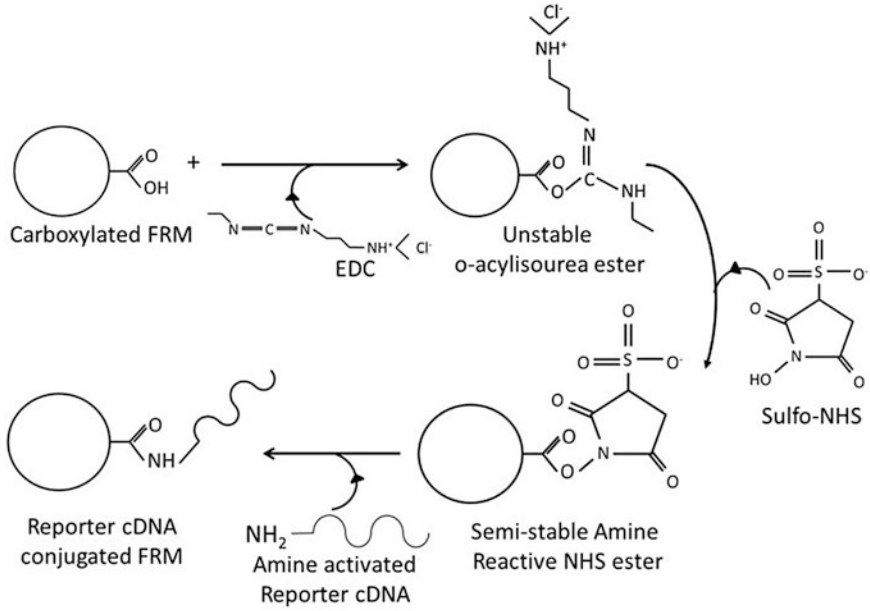

Fig. 2 A schematic of the reactions linking a polystyrene FRM with an amine-linked rDNA. First, the carboxyl on the FRM reacted with EDC to form an o-acylisourea ester, which further reacted with sulfo-NHS to form an amine-reactive NHS ester on the FRM surface. The NHS ester on the FRM surface reacted with the amine at the 5′ end of an rDNA to form a peptide bond to covalently bond the rDNA on the FRM surface

the MPS was proven to be effective to facilitate the immobilization of the probe DNA.

5. A schematic illustrating the immobilization of the amine-activated probe on the PEPS surface via the thiol functionality of the MPS insulation layer is shown in the supplemental information of Reference [3].
6. After probe immobilization, the PEPS was treated with 3% bovine serum albumin (Sigma) in PBS for 1 h followed by washing five times with PBS. As demonstrated by the previous study, 3% BSA was sufficient to completely block nonspecific binding for DNA detection in urine. [3]
7. The MT FRMs were covalently conjugated to MTrDNA and the WT FRMS to the WTrDNA [8, 25] as follows. Both MT FRMs and WT FRMs came capped with carboxyl (−COOH) groups on the surface. To conjugate a FRM with an amine-activated rDNA, the carboxyl on a FRM reacted with EDC to form an immediate o-acylisourea ester, which reacted with sulfo-NHS to form an amine-reactive NHS ester on the FRM surface. The bound NHS ester further reacted with the amine at the 5′ end of the rDNA to form a peptide bond to covalently bond the rDNA to the FRM surface. Figure 2 shows a schematic of these reaction steps.

8. A suspension of MT FRMs, WT FRMs, or an equal mixture of the two was run through the detection cell for 30 min following the detection of MT, WT, or a mixture of MT and WT as a follow-up in situ detection validation. The total volume of the suspension of the mixture of MT FRMs and WT FRMs was 8 mL and the concentration was 1×10^5 FRMs/mL. At 2 mL/min, this suspension was recycled 7.5 times in the 30 min of the MT FRMs and WT FRMs follow-up in situ validation detection step.

3.4 Spiked Urine Samples and Flow Setup

1. The flow system for carrying out the detection contained a peristaltic pump (Cole-Parmer 77,120–62), a custom-made flow cell where detection took place, reservoirs containing DNA-spiked urine samples, FRMs, and PBS interconnected with tubing of a 0.8-mm inner diameter as schematically shown in Fig. 3c.

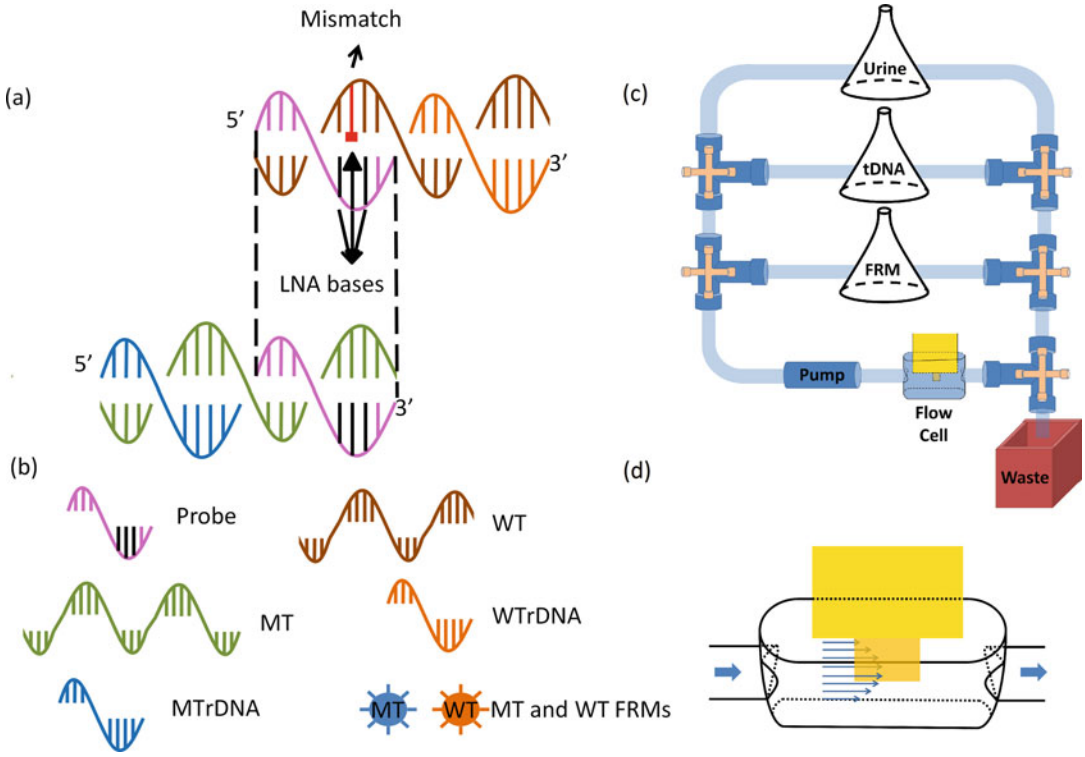

Fig. 3 (**a**) A schematic of the relationship between probe, mutant (MT) target DNA, wild type (WT), MT reporter DNA (MTrDNA), and WT rDNA (WTrDNA) for *KRAS* point mutation, (**b**) the legend for schematic in (**a**), (**c**) a schematic of the flow system for mutation detection in urine and (**d**) a blow-up of the PEPS situated in the center of the flow cell

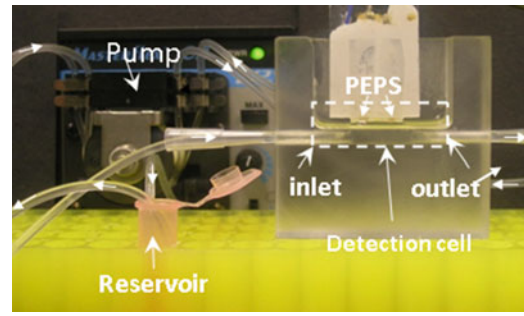

Fig. 4 A photograph of a flow cell machined from a polycarbonate block

2. The flow cell was 18.5 mm long, 3.5 mm wide and 5.5 mm deep (volume = 356 μL) connected to the sample reservoir.
3. A schematic of the flow cell is shown in Fig. 3d. The flow cell was machined from a polycarbonate block. A photograph of a polycarbonate flow cell is shown in Fig. 4. The total internal volume of the flow cell plus tubing was approximately 750 μL.
4. The urine came from one individual. The subject was free of HBV infection. The urine samples were collected in a "First Morning Specimen" manner, i.e., the bladder was emptied before bed and the sample was collected first thing in the morning (*see* **Note 2**). A total of 11 such urine samples were collected for the study and visually there was no significant difference among these 11 urine samples and 21 more that were used for previous studies [3, 43].
5. The flow was driven by the peristaltic pump and what flowed through the flow cell was controlled by the valves.
6. In each detection experiment, the volume of the DNA-spiked urine sample was fixed at 50 mL and the probe-coated PEPS was placed in the center of the flow cell.
7. The flow setup was placed inside an incubator for temperature control.
8. Because the flow cell was open, a 2-L water bath was included in the incubator to eliminate potential resonance frequency shift due to the changes in the flow-cell liquid level by evaporation.
9. The resonance spectra were measured using a portable AIM 4170° C impedance analyzer.

3.5 MT FRMs and WT FRMs Imaging

1. MT FRMs were imaged using a D350/50 filter for excitation and a 400 nm long-pass filter for emission.
2. WT FRMs were imaged by using a D460/50 filter for excitation and a HQ545/30 filter for emission.

3. MT FRMs image were then colored blue to denote that they were MT FRMs using MatLab.
4. WT FRMs image were then colored orange to denote that they were WT FRMs using MatLab.
5. Blue MT FRMs and orange WT FRMs images were merged using MatLab.

3.6 Mutation Detection

1. An optical micrograph of the PEPS used for this study is shown as an insert in Fig. 1c.
2. The in-air and in-PBS phase angle versus frequency resonance spectra of the PEPS are shown in Fig. 1c. As can be seen, the base-line, the length-extension-mode (LEM) resonance peak and the width-extension-mode resonance (WEM) peak of the in-liquid spectrum were close to those of the in-air spectrum, indicating the effectiveness of the MPS insulation coating. In all of the following experiments the WEM peak of the phase-angle spectrum was monitored for detection.
3. The relative resonance frequency shift, $\Delta f/f$, of the first WEM peak during the sulfo-SMCC bonding (30–60 min), the probe immobilization (60–90 min), the subsequent MT detection at 100 pM in PBS (90–120 min) and the following MT FRMs detection at 1×10^5 FRMs/mL concentration in PBS (120–150 min), both a 2 mL/min is shown in Fig. 1d. Also shown in the insert in Fig. 1d is a schematic of the various steps involved in the immobilization process. The data depicted in Fig. 1d was generated using PBS at room temperature in order to illustrate that the various binding steps during surface functionalization, MT detection or FRM validation could be detected by the resonance frequency shift of the PEPS. For actual MT or WT detection in urine, there was a bovine serum albumin (BSA) blocking step right after probe immobilization in which the probe-coated PEPS was soaked in a 3% BSA solution for 30 min right before detection in urine to saturate any possible nonspecific binding sites such that no nonspecific binding could occur during detection in urine as described earlier [3].
4. With the melting temperature for the binding of the MT to the probe being 70 °C and that for the WT to the probe being 55 °C, we carried out the detection of 1×10^{-15} M of MT and WT in PBS at 55 °C, 60 °C, 63 °C, and 68 °C for 30 min to find the optimal temperature for specific MT detection against the WT. Three experiments were carried for each condition as described above (*see* **Note 3**). The resultant relative detection resonance frequency shift, $\Delta f/f$ is plotted with standard deviations in Fig. 1e. We then averaged out the $\Delta f/f$ of each detection over 25–30 min. The resultant $-\Delta f/f$ at 25–30 min is

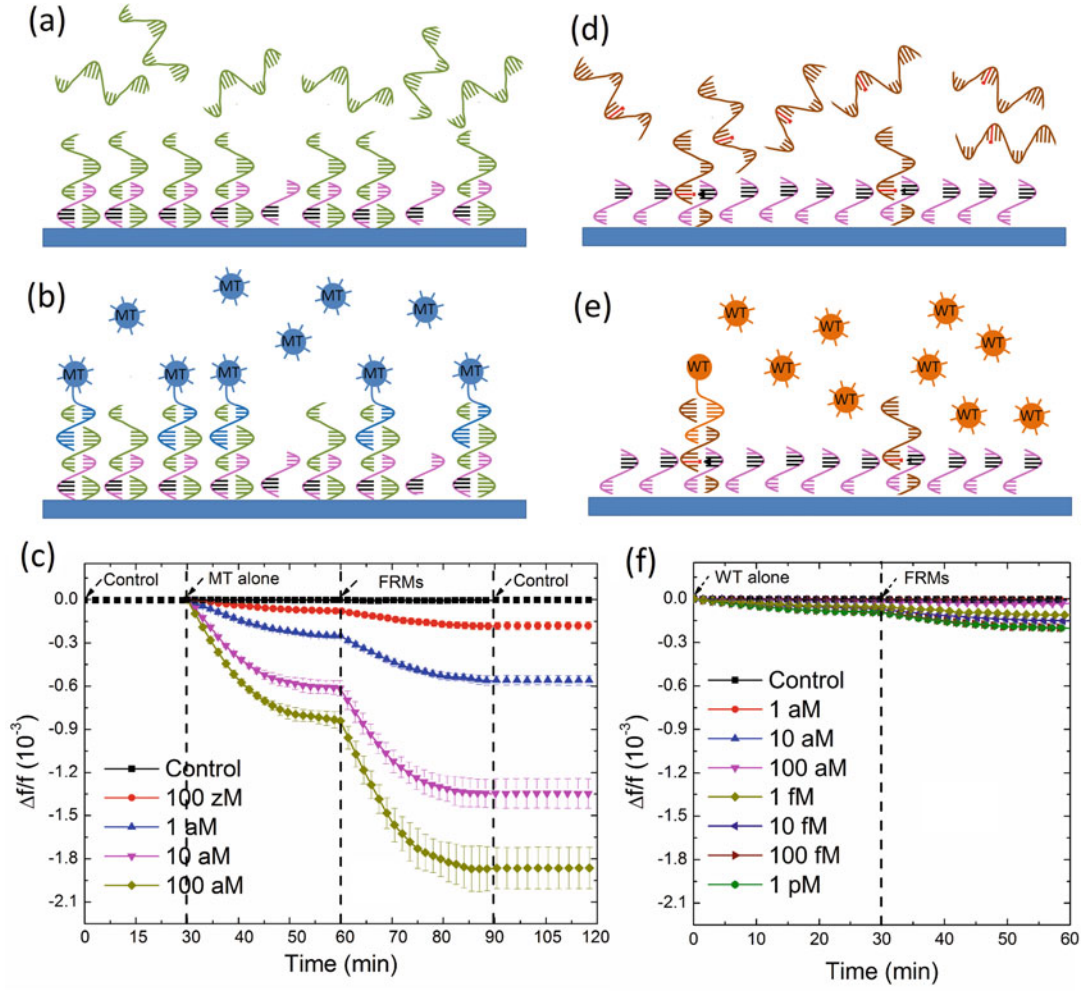

Fig. 5 A schematic representation of (**a**) MT detection (**b**) MT FRMs detection following MT detection, (**c**) Δf/f versus time of MT detection followed by MT FRMs detection including the background signal collection in urine before (0–30 min) and after (90–120 min) the MT and FRMs detection, (**d**) WT detection (**e**) WT FRMs detection following WT detection, (**f**) Δf/f versus time of WT detection followed by WT FRMs detection. Clearly, at 63 °C and at a flow rate of 4 mL/min, the detection $-\Delta f/f$ of 1 aM MT at $t = 30$ min ($-\Delta f/f = 0.2 \times 10^{-3}$) was much larger than that of WT at 100 f. at $t = 30$ min, ($-\Delta f/f < 0.1 \times 10^{-3}$), indicating the specificity of the MT detection at such detection conditions

plotted in Fig. 1f with squares representing MT and circles representing WT (the left side of the double-y plot). The ratio of the $-\Delta f/f$ at 25–30 min of the MT to that of the WT is also plotted in Fig. 1f as the triangles (the right side of the double-y plot). As can be seen the ratio of the $-\Delta f/f$ at 25–30 min of the MT to that of the WT was maximal at 63 °C.

5. Figure 5a, b show the schematic of the MT detection in urine in which MT containing urine flowed through the detection cell and that of the following MT FRMs detection in which the MT

FRMs containing PBS flowed through the detection cell, respectively. Figure 5c shows the detection Δf/f versus time of the MT detection in urine at various MT concentrations followed by the MT FRMs detection in PBS at 1×10^5 FRMs/mL. Note the background signal in blank urine (control) before and after the MT and FRM detection steps were stable as shown in Fig. 5c in all the detection experiments. For simplicity, in all the following figures we will omit the background signal sections to better highlight the detection results.

6. Figure 5d, e show the schematic of the WT detection in urine and that of the following detection of the WT FRMs in PBS, respectively.
7. Figure 5f shows the detection $-\Delta f/f$ versus time in urine at various MT concentrations followed by the detection of the WT FRMs in PBS at 1×10^5 FRMs/mL. Clearly, the detection $-\Delta f/f$ for MT at 1 aM (1×10^{-18} M) at $t = 30$ min was about 0.2×10^{-3}, which was still larger than the detection $-\Delta f/f$ of $<0.1 \times 10^{-3}$ for WT at 100 f. (1×10^{-14} M) at $t = 30$ min, indicating the specificity of the MT detection by PEPS at the chosen detection conditions of 63 °C and 4 mL/min flow rate.
8. To see if PEPS detection of *KRAS* MT under the current detection conditions, i.e., 63 °C and a flow rate of 4 mL/min was indeed sensitive and specific, we carried out MT detection in a background of 1000-fold higher WT at various MT concentrations.
9. In Fig. 6a, we show the Δf/f versus time of PEPS detection in urine containing a mixture of MT in a background of 1000-fold more WT at various MT concentrations followed by detection in an equal mixture of 10^5 FRMs/mL of MT FRMs and 10^5 FRMs/mL of WT FRMs in PBS.
10. After the detection in the mixture of MT FRMs and WT FRMs and washing, the PEPS was examined using a fluorescent microscope and the obtained fluorescent images from detection at various MT concentrations as described in Subheading 3.5 are shown in Fig. 6b–e where the blue spots represent the MT FRMs and the orange ones WT FRMs. As can be seen, in all four MT concentrations (i.e., 100 zM, 1 aM, 10 aM, and 100 aM) the blue MT FRMs outnumbered the orange WT FRMs. In addition, both the number of MT FRMs and that of the WT FRMs increased with an increasing MT concentration since the WT concentration was increased in proportion as well.
11. In Fig. 7a, we plot the number of MT FRMs and that of WT FRMs versus the average $-\Delta f/f$ of MT detection in a MT/WT mixture as obtained from the $-\Delta f/f$ at $t = 25$–30 min in Fig. 6a. Clearly, both the number of the MT FRMs and that of the WT

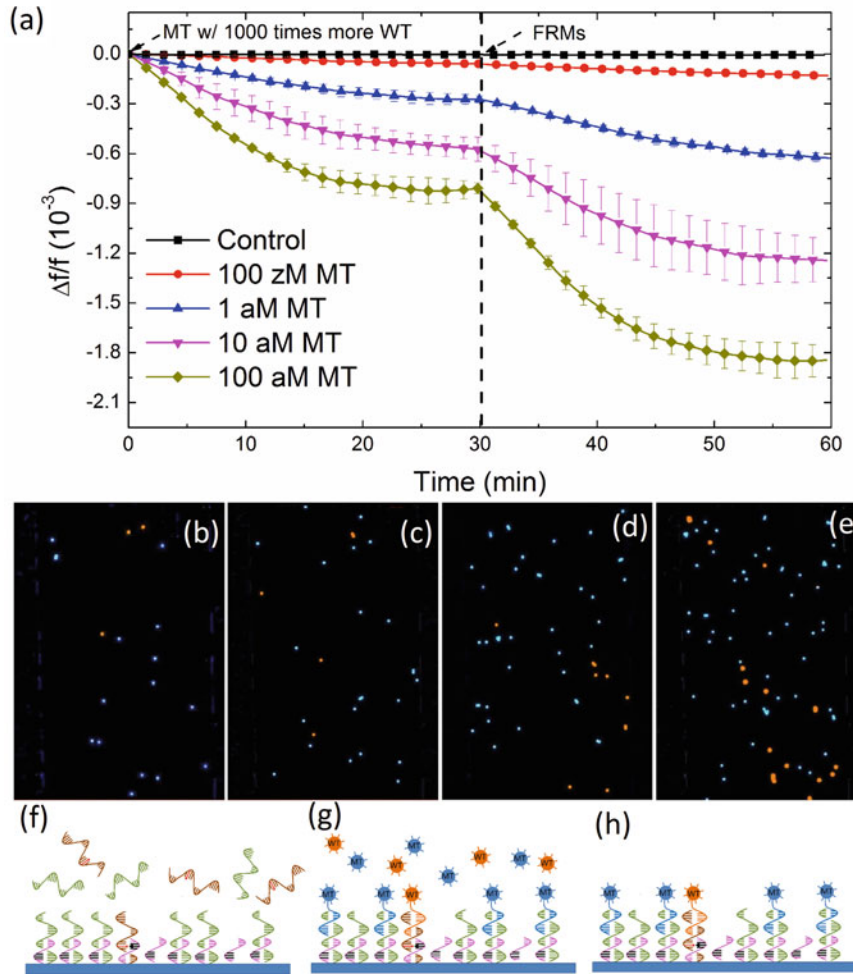

Fig. 6 (**a**) Relative resonance frequency shift, Δf/f versus time of PEPS detection of MT in a background of 1000-fold more WT at various MT concentrations followed by detection in an equal mixture of 10^5 FRMs/mL of MT FRMs and 10^5 FRMs/mL of WT FRMs in PBS, (**b**), (**c**), (**d**), and (**e**) are respectively the fluorescent images of the PEPS obtained after the FRMS detection following the MT detections at 0.1 aM (100 zM), 1 aM, 10 aM, and 100 aM MT concentrations where the *blue* color denotes the MT FRMs while the *orange* color denotes the WT FRMs, (**f**), (**g**), and (**h**) are respectively the schematic illustrating the PEPS in a mixture of MT and WT at t=0–30 min in (**a**), a schematic of the PEPS in a mixture MT FRMs and WT FRM at t= 30–60 min in (**a**), and a schematic of the PEPS after the final washing. That there were far more MT FRMs captured than WT FRMs in (**b**–**e**) indicates that the detection of MT was specific even in a background of 1000 times more WT

FRMs increased roughly linearly with an increasing average −Δf/f of MT detection with a MT FRMs/WT FRMs number ratio of about 4, validating that the Δf/f obtained in a MT/WT mixture with a WT/MT ratio of 1000 was mostly due to the binding of MT on the PEPS surface such that the bound FRMs were mostly MT FRMs. These results are schematically illustrated in Figs. 6f–h. Figure 6f illustrates that even in a mixture

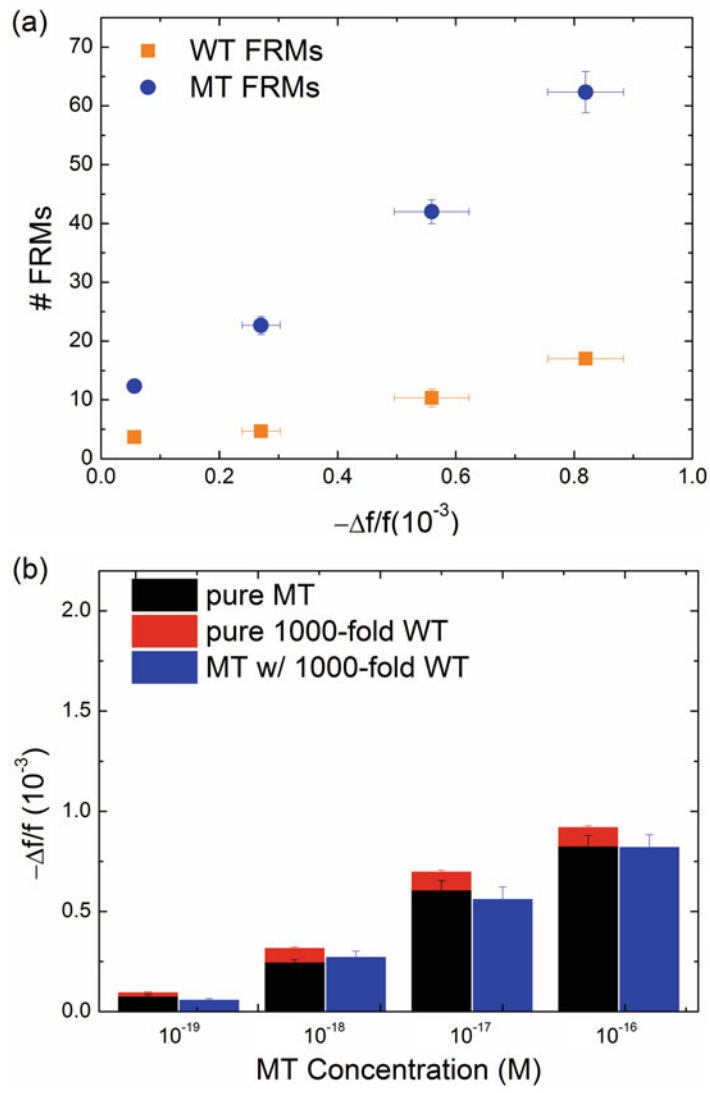

Fig. 7 (**a**) Number of MT FRMs (*blue full circles*) and that of WT FRMs (*orange full squares*) obtained from Figs. 6b–e versus average PEPS MT detection $-\Delta f/f$ at $t = 25$–30 min taken from Fig. 6a. Note for each MT concentration the number of MT FRMs (*blue*) was still roughly four times higher than that of the WT even the concentration of the WT was 1000 times higher than that of the MT. This indicates that in each case more than 80% of the detection $\Delta f/f$ was due to the binding of the MT and that PEPS's MT detection was specific even the concentration of the WT was 1000 times higher than that of the MT. (**b**) Comparison of $-\Delta f/f$ for detection averaged over $t = 25$–30 min of pure MT in Fig. 6c (*black*), that at 1000-fold pure WT taken from Fig. 6f (*red*) and that in a mixture of MT in 1000-fold more WT as taken from Fig. 7a (*blue*). That the $-\Delta f/f$ in a mixture of MT in 1000-fold (*blue*) was similar to the sum of the $-\Delta f/f$ of MT and the $-\Delta f/f$ of 1000-fold WT more WT indicates that the presence of the 1000-fold WT had negligible effect on the MT detection. In addition, that the $-\Delta f/f$ of pure MT (*black*) was also roughly four times that of 100-fold pure WT (*red*), further confirming the specificity of the current PEPS single-nucleotide mutation detection

of MT with 1000-fold more WT, still more MT than WT were captured on the PEPS surface because the temperature and flow condition favored MT to bind to the probe on the PEPS surface.

12. Figure 6g illustrates that in detection in an equal mixture of MT FRMs and WT FRMs following the detection in the mixture of MT with 1000-fold more WT, more MT FRMS would bond on the PEPS surface due to more MT captured on the PEPS surface.
13. Figure 6h illustrates that the final PEPS surface had more bound MT FRMs with a MT FRMs/WT FRMs number ratio of about 4 after detection in the equal mixture of MT FRMs and WT FRMs and washing.
14. To see how the detection of MT in a background of 1000-fold WT shown in Fig. 6a compared with detection in pure MT and that in pure WT in Fig. 5c, f, we plot in Fig. 7b the average $-\Delta f/f$ over $t = 25$–30 min at 10^{-19} M, 10^{-18} M, and 10^{-17} M in pure MT (black) as obtained from Fig. 5c, that at 1000-fold WT (red) as obtained from Fig. 5f, and that in a mixture of MT with 1000-fold WT (blue) as obtained from Fig. 6a (blue). As can be seen from Fig. 7b, the overall detection $-\Delta f/f$ in a mixture (blue) was somewhat smaller than that of pure MT detection at the same concentration (black), understandably due to the interference by the presence of the 1000-fold WT except at low concentrations where WT had a negligible effect due to the low concentrations (*see* **Note 4**).
15. Note in Fig. 7b, the $-\Delta f/f$ of the pure MT detection (black) of all three concentrations were also roughly four times that of the pure WT detection at a 1000-fold higher concentration, consistent with the results from the detection in MT/WT mixture shown in Fig. 7a and further supporting that under the detection conditions of 63 °C and 4 mL/min, roughly 80% (4 out of 5) of the detection signals were due to MT even in a background of 1000-fold WT.
16. In Summary, we have examined the analytical sensitivity and selectivity of in situ detection of gene mutation in urine using a PMN-PT PEPS using *KRAS* G12 V point mutation (PM) as the model PM. The PEPS was coated with a 17-nt probe with three LNA bases around the mutated site that was complementary to the *KRAS* PM and the detection was carried out in a flow with the PEPS located at the center of the flow with a flow rate of 4 mL/min and at 63 °C which was below the melting temperature of the MT with the probe but above that of the WT with the probe (*see* **Note 5**). The specificity of the mutation detection in a background of wild type was examined in situ by following with the detection in a mixture of blue MT FRMs

and orange WT FRMs and further confirmed by visual inspection of the colors of the bound FRMs. We showed that even in a background of 1000-fold wild type PEPS specifically detected the *KRAS* PM with an analytical sensitivity of 60 copies/mL in urine without DNA isolation or amplification, which was validated by the fact that the captured blue MT FRMs still outnumbered the orange WT FRMs 4 to 1 even the WT outnumbered the MT by 1000-fold (*see* **Note 6**).

4 Notes

1. Given that the current probe was only 17-nt long with the mutated site in the middle (9th-nt), as long as the mutation site of a target MT is 8-nt or more from the edge of the target DNA, the binding of the probe to the target MT will have the expected melting temperature of 70 °C.
2. In urine most of the tumor derived cell free DNA fragments are low molecular weight (200 bp) [23]. The probability for the mutated site to be within 8 nt of either end would therefore be less than 8% on average. Thus, the current 17-nt probe would bind to the DNA fragments in urine with a probability of better than 92%.
3. The current hybridization temperature is not high enough to denature dsDNA. Detection of dsDNA will require denaturing the dsDNA prior to hybridization, which can be incorporated in the flow system in a continuous fashion and will be published in future publication.
4. In comparison, PCR needs two primers and one probe, thus would not be able to detect a MT with a mutation site as far off the center as 8 nt away from the edge. Conservatively assuming the two primers and the probe to be all 17-nt long, for the MT to be detectable, the mutation site must be 25-nt or more away from the edge, reducing the chances of detecting the MT to 75%. Most of the primer and probe sequences in PCR are much longer than 17-nt long, which will further reduce the chance of detecting the mutation from the fragments. Clearly, the current method needs only a short probe is an advantage over PCR in detecting mutations from circulating DNA fragments.
5. Finally, the PEPS mutation detection method can be easily adopted for one-step multiplexed in situ mutations detection as illustrated for by simultaneous detection of the six codon 12 KRAS mutations in one single test [10].
6. The same methodology should also be able to detect mutations in circulating DNA from plasma or serum. The only difference is

that the sensor must be blocked with a higher concentration of bovine serum albumin (BSA) after probe immobilization and prior to detection to prevent nonspecific binding as plasma and sera contain higher concentrations of serum albumin [42].

Acknowledgment

This work was supported in part by the Coulter-Drexel Translational Research Partnership grant, the Nanotechnology Institute of Benjamin Franklin Partnership of Southeastern Pennsylvania, and National Institute of Health Grants No. R41AI112224 and R41AI120445.

References

1. Shih WY, Luo HY, Li HD, Martorano C, Shih WH (2006) Sheet geometry enhanced giant piezoelectric coefficients. Appl Phys Lett 89. doi:10.1063/1.2408633 Artn 242913
2. Luo H, Shih WY, Shih WH (2007) Double precursor solution coating approach for low-temperature sintering of [Pb(Mg1/3Nb2/3)O-3](0.63)[PbTiO3](0.37) solids. J Am Ceram Soc 90:3825–3829. doi:10.1111/j.1551–2916.2007.02072.x
3. Kirimli CE, Shih WH, Shih WY (2014) DNA hybridization detection with 100 zM sensitivity using piezoelectric plate sensors with an improved noise-reduction algorithm. Analyst 139:2754–2763. doi:10.1039/c4an00215f
4. Zhu Q, Shih WY, Shi WH (2009) Enhanced detection resonance frequency shift of a piezoelectric microcantilever sensor by a DC bias electric field in humidity detection. Sens Actuators B-Chem 138:1–4. doi:10.1016/j.snb.2009.01.035
5. Zhu Q, Shih WY, Shih WH (2008) Mechanism of flexural resonance frequency shift of a piezoelectric microcantilever sensor during humidity detection. Appl Phys Lett 92. doi:10.1063/1.2921050 Artn 183505
6. Shih WY, Zhu Q, Shih WH (2008) Length and thickness dependence of longitudinal flexural resonance frequency shifts of a piezoelectric microcantilever sensor due to Young's modulus change. J Appl Phys 104. doi:10.1063/1.2990057 Artn 074503-074503-5
7. Zhu Q, Shih WH, Shih WY (2013) Enhanced dimethyl methylphosphonate (DMMP) detection sensitivity by lead-magnesium niobate-lead-titanate/copper piezoelectric microcantilever sensors via Young's modulus change. Sens Actuators B-Chem 182:9
8. Wu W, Kirimli CE, Shih WH, Shih WY (2013) Real-time, in situ DNA hybridization detection with attomolar sensitivity without amplification using (pb(Mg1/3Nb2/3)O-3)(0.65)-(PbTiO3)(0.35) piezoelectric plate sensors. Biosens Bioelectron 43:391–399. doi:10.1016/j.bios.2012.12.044
9. Wu W, Shih WY, Shih W-H (2016) eEnhancing detection sensitivity of piezoelectric plate sensor by increasing transverse electromechanical coupling constant. J Appl Phys 114:064505
10. Kirimli CE, Shih WH, Shih WY (2016) Amplification-free in situ KRAS point mutation detection at 60 copies per mL in urine in a background of 1000-fold wild type. Analyst 141:1421–1433. doi:10.1039/c5an02048d.
11. Bauer S, Bauer F (2008) Piezoelectricity. In: Heywang W, Lubitz K, Wersing W (eds) Evolution and future of a technology. Springer-Verlag, Berlin, Heidelberg, pp 161–164
12. Zhu Q, Shih WY, Shih WH (2007) Real-time, label-free, all-electrical detection of Salmonella typhimurium using lead titanate zirconate/gold-coated glass cantilevers at any relative humidity. Sens Actuators B-Chem 125:379–388. doi:10.1016/j.snb.2007.02.030
13. Zhu Q, Shih WY, Shih WH (2007) In situ, in-liquid, all-electrical detection of Salmonella typhimurium using lead titanate zirconate/gold-coated glass cantilevers at any dipping depth. Biosens Bioelectron 22:3132–3138. doi:10.1016/j.bios.2007.02.005
14. Zheng S, Choi JH, Lee SM, Hwang KS, Kim SK, Kim TS (2011) Analysis of DNA hybridization regarding the conformation of molecular layer with piezoelectric microcantilevers.

Lab Chip 11:63–69. doi:10.1039/C0lc00122h

15. Shen ZY, Shih WY, Shih WH (2006) Self-exciting, self-sensing PbZr0.53Ti0.47O3/SiO2 piezoelectric microcantilevers with femtogram/Hertz sensitivity. Appl Phys Lett 89. doi:10.1063/1.2219994 Artn 023506
16. Lee JH, Kim TS, Yoon KH (2004) Effect of mass and stress on resonant frequency shift of functionalized Pb(Zr0.52Ti0.48)O-3 thin film microcantilever for the detection of C-reactive protein. Appl Phys Lett 84:3187–3189. doi:10.1063/1.1712028
17. Rijal K, Mutharasan R (2007) PEMC-based method of measuring DNA hybridization at femtomolar concentration directly in human serum and in the presence of copious noncomplementary strands. Anal Chem 79:7392–7400. doi:10.1021/Ac0712042
18. Crowley E, Di Nicolantonio F, Loupakis F, Bardelli A (2013) Liquid biopsy: monitoring cancer-genetics in the blood. Nat Rev Clin Oncol 10:472–484. doi:10.1038/nrclinonc.2013.110
19. Robertson EG, Baxter G (2011) Tumour seeding following percutaneous needle biopsy: the real story! Clin Radiol 66:1007–1014. doi:10.1016/j.crad.2011.05.012
20. Lipsky RH, Mazzanti CM, Rudolph JG et al (2001) DNA melting analysis for detection of single nucleotide polymorphisms. Clin Chem 47:635–644
21. Caruso F, Rodda E, Furlong DN, Niikura K, Okahata Y (1997) Quartz crystal microbalance study of DNA immobilization and hybridization for nucleic acid sensor development. Anal Chem 69:2043–2049. doi:10.1021/ac961220r
22. Su YH, Wang M, Block TM et al (2004) Transrenal DNA as a diagnostic tool: important technical notes. Ann N Y Acad Sci 1022:81–89
23. Su YH, Wang MJ, Brenner DE et al (2004) Human urine contains small, 150 to 250 nucleotide-sized, soluble DNA derived from the circulation and may be useful in the detection of colorectal cancer. J Mol Diagn 6:101–107. doi:10.1016/S1525-1578(10)60497-7
24. Umansky SR, Tomei LD (2006) Transrenal DNA testing: progress and perspectives. Expert Rev Mol Diagn 6:153–163
25. Kirimli CE, Shih WH, Shih WY (2013) Temperature- and flow-enhanced detection specificity of mutated DNA against the wild type with reporter microspheres. Analyst 138:6117–6126. doi:10.1039/c3an00384a
26. Kirimli CE, Shih WH, Shih WY (2015) Specific in situ hepatitis B viral double mutation (HBVDM) detection in urine with 60 copies ml(−1) analytical sensitivity in a background of 250-fold wild type without DNA isolation and amplification. Analyst 140:1590–1598. doi:10.1039/c4an01885k
27. Bazan V, Agnese V, Corsale S et al (2005) Specific TP53 and/or Ki-ras mutations as independent predictors of clinical outcome in sporadic colorectal adenocarcinomas: results of a 5-year gruppo oncologico dell'Italia meridionale (GOIM) prospective study. Ann Oncol 16 (Suppl 4):iv50–iv55
28. Eser S, Schnieke A, Schneider G, Saur D (2014) Oncogenic KRAS signalling in pancreatic cancer. Br J Cancer 111:817–822. doi:10.1038/bjc.2014.215
29. Imamura Y, Morikawa T, Liao X et al (2012) Specific mutations in KRAS codons 12 and 13, and patient prognosis in 1075 BRAF wild-type colorectal cancers. Clin Cancer Res 18:4753–4763
30. Forbes SA, Bindal N, Bamford S et al (2011) COSMIC: mining complete cancer genomes in the catalogue of somatic mutations in cancer. Nucleic Acids Res 39:D945–D950. doi:10.1093/nar/gkq929
31. Ugozzoli LA, Latorra D, Puckett R, Arar K, Hamby K (2004) Real-time genotyping with oligonucleotide probes containing locked nucleic acids. Anal Biochem 324:143–152
32. Chou LS, Meadows C, Wittwer CT, Lyon E (2005) Unlabeled oligonucleotide probes modified with locked nucleic acids for improved mismatch discrimination in genotyping by melting analysis. Biotechniques 39:644 6, 8 passim
33. Johnson MP, Haupt LM, Griffiths LR (2004) Locked nucleic acid (LNA) single nucleotide polymorphism (SNP) genotype analysis and validation using real-time PCR. Nucleic Acids Res 32:e55. doi:10.1093/nar/gnh046
34. Kierzek E, Ciesielska A, Pasternak K, Mathews DH, Turner DH, Kierzek R (2005) The influence of locked nucleic acid residues on the thermodynamic properties of 2'-O-methyl RNA/RNA heteroduplexes. Nucleic Acids Res 33:5082–5093. doi:10.1093/nar/gki789
35. Koshkin AA, Singh SK, Nielsen P et al (1998) LNA (Locked Nucleic Acids): synthesis of the adenine, cytosine, guanine, 5-methylcytosine, thymine and uracil bicyclonucleoside monomers, oligomerisation, and unprecedented nucleic acid recognition. Tetrahedron 54:3607–3630 http://dx.doi.org/10.1016/S0040-4020(98)00094-5

36. Orum H, Jakobsen MH, Koch T, Vuust J, Borre MB (1999) Detection of the factor V Leiden mutation by direct allele-specific hybridization of PCR amplicons to photoimmobilized locked nucleic acids. Clin Chem 45:1898–1905
37. Simeonov A, Nikiforov TT (2002) Single nucleotide polymorphism genotyping using short, fluorescently labeled locked nucleic acid (LNA) probes and fluorescence polarization detection. Nucleic Acids Res 30:e91
38. Tolstrup N, Nielsen PS, Kolberg JG, Frankel AM, Vissing H, Kauppinen S (2003) OligoDesign: Optimal design of LNA (locked nucleic acid) oligonucleotide capture probes for gene expression profiling. Nucleic Acids Res 31:3758–3762
39. Land MA, Webster J, Christoforou A et al (2014) Salt intake assessed by 24 h urinary sodium excretion in a random and opportunistic sample in Australia. BMJ Open 4:e003720. doi:10.1136/bmjopen-2013-003720
40. Dugdale DC (2017) Urine Output in MDhealth. http://www.md-health.com/Normal-Urine-Output.html. Accessed 17 Feb 2017
41. Soylu MC, Shih W-H, Shih WY (2013) Insulation by Solution 3-Mercaptopropyltrimethoxysilane (MPS) coating: effect of pH, water, and MPS content. Ind Eng Chem Res 52:2590–2597
42. Soylu MÇ (2013) Piezoelectric plate sensor for in situ genetic detection of hepatitis B virus in serum without DNA isolation and amplification. Drexel University
43. Kirimli CE, Shih W-H, Shih WY (2015) Specific in situ hepatitis B viral double mutation (HBVDM) detection in urine with 60 copies/ml analytical sensitivity in a background of 250-fold wild type without DNA isolation and amplification. Analyst 140(5):1590–1598. doi:10.1039/C4AN01885K